Simulation of STM images of three-dimensional surfaces and comparison with experimental data: Carbon nanotubes

Géza I. Márk,* László P. Biró, and József Gyulai
KFKI, Research Institute for Technical Physics and Materials Science, H-1525 Budapest, P.O. Box 49, Hungary
(Received 12 December 1997; revised manuscript received 8 May 1998)

Computer simulation by numerically solving the time-dependent Schrödinger equation was used to investigate image formation during scanning tunneling microscope (STM) imaging of three-dimensional objects with radii of curvature comparable with that of the STM tip. The results were compared with experiment. When the nanotube is placed on a substrate with similar electronic structure, the only distortion arises from geometric convolution. When the substrate and the nanotube have different electronic structures, additional distortions arise. The time evolution of the tunneling process shows that in the interpretation of the scanning tunneling spectroscopy data one has to take into account the nanotube not being an integral part of the underlying substrate. [S0163-1829(98)01140-0]

Carbon nanotubes (NT's) are a new class of nano-objects with remarkable physical, chemical, and mechanical properties.[1] Their electronic properties depend on the way in which the graphene layer is rolled to a cylinder, and on the diameter of the tubule.[1,2] Due to its versatility in studying objects with nm size, the scanning tunneling microscope (STM) has been widely used to investigate carbon NT's.[3–9] The STM is able to acquire by STS data regarding the electronic structure of a single NT.[3,9] Some differences arise in the STM imaging of a three-dimensional object ''floating'' over the surface of the support as compared with single crystalline surfaces. In this case one cannot neglect the convolution effects arising at the very end of the STM tip. This will produce an apparent broadening of the NT.[10] The existence of two tunneling gaps: between the tip and the NT; and between the NT and the surface over which it is floating, and the differences in the electronic structure of the NT and that of the support may have a significant effect on the tunneling current. We use computer simulation to investigate these effects and to compare experimental data with the simulation results. Two sets of experimental data published earlier will be analyzed: (i) the NT is placed on a support with identical physical properties, i.e., we analyze a NT on a ''raft,''[10] and (ii) the NT is placed on highly oriented pyrolytic graphite (HOPG).[11] As a first approximation, we calculated the image distortions caused by finite tip size using a geometric method. Hereafter this is referred as ''geometric line cut'' (GLC). To check the validity of the GLC quantum-mechanical probability current calculations were performed through a two-dimensional (2D) jellium potential. Hereafter this is referred to as a ''quantum line cut'' (QLC).

The model system is shown in the inset of Fig. 1. The NT is modeled by a cylinder of 0.5 nm radius floating above the support at a distance of 0.335 nm. This is the distance of the graphene sheets in HOPG and similar distances have been found between the elements of the single wall carbon NT ropes.[12] The STM tip is approached by a rotational hyperboloid of 0.5 nm apex radius and 15° aperture angle. The effective surface of the electrodes is assumed to be 0.071 nm outside the geometric surface. This is the half-nearest-neighbor distance in HOPG. The GLC is shown in Fig. 1 by a solid line. It is defined as the line drawn by the tip apex point (X_{apex}, Z_{apex}), when the distance of the nearest point of the sample and tip effective surfaces is constant. This constant is chosen to be 0.4093 nm to allow a direct comparison with the QLC (see below) at $X_{apex}=0$. When the tip is far from the NT the line cut is a horizontal line above the support surface. When the tip approaches the NT the nearest tip point to the sample shifts from the apex to a point on the side of the tip.

The quantum-mechanical tunneling probability is calculated from the time-dependent scattering of a wave packet (WP) on the effective potential modeling the system. This conceptionally simple and easy to implement method contains no perturbative approximation but includes all interference[13] and multiple scattering effects and thus it is capable of providing results comparable with the most recent

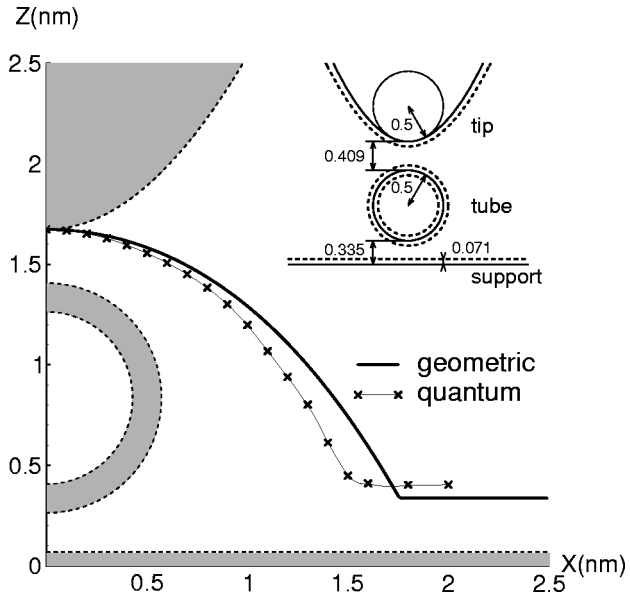

FIG. 1. Geometric and quantum line cuts. The thick line is the GLC drawn by the tip apex. The shaded lower half-plane, middle ring, and upper hyperbola show the vertical cross sections of the support, NT, and tip, respectively. The electrodes are bounded by their effective surfaces (broken lines). Crosses show calculated points of the QLC. A thin solid line connecting the crosses was drawn to guide the eye. Model system geometry is displayed in the inset. All dimensions are in nm. The effective surface (broken line) is 0.071 nm outside of the geometric surface (full line).

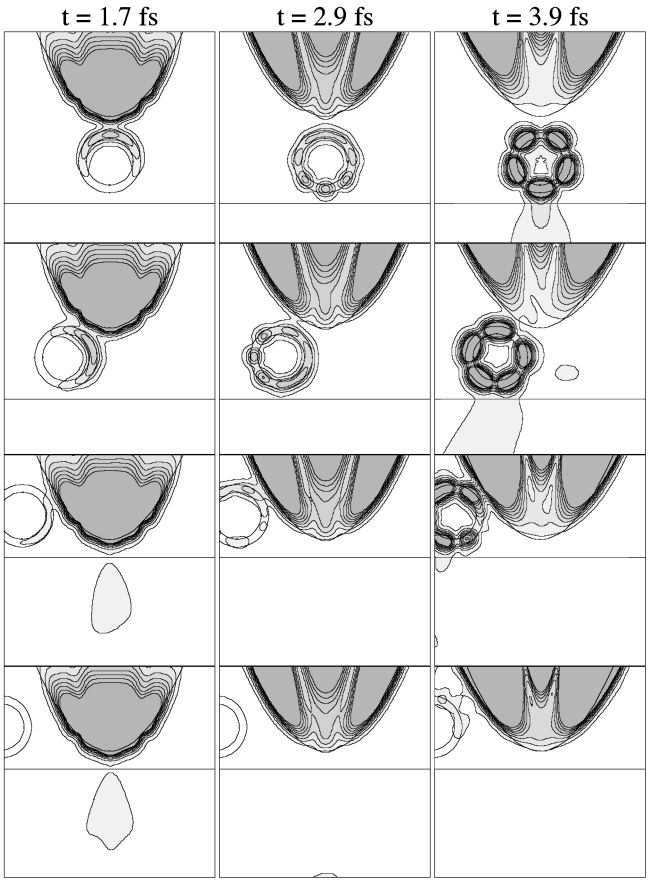

FIG. 2. Probability density of the scattered wave packet for selected time instants and X_{apex} lateral tip displacements (0.0, 0.8, 1.6, and 2.0 nm). Size of the presentation window is 3.84 nm. Contour lines are drawn on sqare root scale. Each frame is normalized to its maximum density. Maximum density values are 4.2, 0.6, and 0.07 nm^{-2} for 1.7, 2.9, and 3.9 fs, respectively. Density in the tube region becomes appreciable on the lower right frame because of the renormalization.

tunneling theories[14] when applying a properly chosen model potential. Inclusion of multiple scattering and interference effects is important for modeling the resonant tunneling process arising because of the existence of two tunnel gaps. The snapshots of the WP probability density shown in Fig. 2 and the tunneling time values of Table I demonstrate the power of the time-dependent method in gaining insight into the details of the tunneling process. In the present paper we use some additional approximations analyzed below.

While it is possible to include realistic atomic structure into the model without any conceptional difficulty through a suitable effective potential, here we are focussing on pure geometrical effects which are well described by a jellium potential. As was shown recently[15] the self-consistent electronic structure of NT's represented by the 2D jellium background model compares favorably with parametrized LCAO calculations that take atomic structure into account. The absence of atomic structure in the jellium tubes is equivalent to averaging over all chiral angles. Our model potential is *zero* outside the effective surfaces of the electrodes and -9.81 eV inside. This is calculated from the HOPG $E_F = 5$ eV Fermi energy[16] and $W = 4.81$ eV work function.[17] This model potential does not account for the different material properties of the tip, NT, and support, it allows the calculation of the influence of the geometry on the tunneling current only and this makes it possible to compare directly the geometric and quantum line cuts. The infinitesimally small bias approximation is justified by the fact that in the experiments analyzed here small bias values were used. Because of the limited computational facilities we calculated only in 2D. The electrostatic potential of the rotationally symmetric tip and the spread of the charge along the tube, which may be important for metallic tubes cannot be accounted for. The net effect is that the 2D model overestimates the tip-tube conductance as compared to the tube-support conductance because it does not take into account that the tip-tube tunnel junction is zero dimensional but the tube-support tunnel junction is one dimensional.

TABLE I. Average time t_{spent} (in *fs*) the quantum particle spends in the different regions. ''Forbidden'' region is the region of zero potential. ''Total interface'' region is the union of the ''forbidden'' and ''tube'' regions.

X_{apex} (nm)	Forbidden	Tube	Total Interface
0.0	0.071	0.084	0.155
0.8	0.079	0.123	0.202
1.6	0.060	0.020	0.080
2.0	0.057	0.0001	0.057

Under the assumptions given in Ref. 14, the tunneling current from the tip to the support for an infinitesimally small bias is proportional to $\Sigma_{mm'} T_{m'm}(E)$, where $T_{m'm}(E)$ is the probability of transmitting an electron from the $|u_t^{-m}(E)\rangle$ tip state to the $|u_s^{-m'}(E)\rangle$ support state. Because at infinitesimal bias only the states near the Fermi energy contribute to the tunnel current, we can estimate $\Sigma_{mm'} T_{m'm}(E)$ by the transmission probability $P_{Gaussian}(E_F)$ of a Gaussian WP having mean energy E_F and a lateral spread $\Delta x \gg HW_T$ where HW_T is the largest half-width of the tunneling channel. (In atomic resolution STM measurement HW_T is approximately $0.1-0.2$ nm. We used $\Delta x = \Delta z = 0.37$ nm.)

The $\psi(\vec{r},t)$ wave function is calculated from the time-dependent 2D Schrödinger equation. The *split operator Fourier transform method*[18–20] was used. In this method the time evolution operator $\exp(-i\mathbf{H}\Delta t)$ is approximated (in Hartree atomic units) by the symmetrical unitary product $\exp(-i\mathbf{K}/2\Delta t)\exp(-i\mathbf{V}\Delta t)\exp(-i\mathbf{K}/2\Delta t)$. While the effect of the potential energy propagator $\exp(-i\mathbf{V}\Delta t)$ is a simple multiplication with $\exp(-iV(\vec{r})\Delta t)$ for local potentials, the effect of the kinetic energy propagator $\exp(-i\mathbf{K}/2\Delta t)$ is given in k space by multiplicating the $\varphi(\vec{k},t)$ momentum space wave function by $\exp(i|\vec{k}|^2/4\Delta t)$. To utilize this formula it is necessary to calculate the $\varphi(\vec{k},t)$ momentum space wave function by fast Fourier transform (FFT) of $\psi(\vec{r},t)$. Finally we have to return back to real space by inverse FFT. The spatial and temporal sampling was chosen according to Ref. 21. The FFT introduces an artificial periodic boundary condition leading to unphysical interference effects among the neighboring cells. To prevent these, we choose a calculation mesh four times bigger ($L_{calc} = 15.36$ nm, 512 points) then

the presentation window ($L_{present}=3.84$ nm, 128 points) and the edges of the calculation mesh were closed by a drain (negative imaginary) potential.

$P_{Gaussian}(E_F)$ is calculated as follows. The $\vec{j}(x,z,t)$ probability current density is calculated along a horizontal line inside the support bulk (at $z_j=-0.5$ nm) from $\psi(x,z,t)$ for all time instants. Line integration of $\vec{j}(x,z,t)$ along this line gives the $I(t)$ probability current and the tunneling probability is $P_{Gaussian}(E_F)=\int_0^{t_{max}} I(t)dt$. Calculation is performed until the further change of $P_{Gaussian}$ becomes negligible. The probability density of the scattered WP is shown on Fig. 2 for selected time instants and X_{apex} lateral tip displacements. (The corresponding Z_{apex} vertical tip displacements are calculated using the method described below.) The average time the quantum particle spends[22] in the different regions of space,

$$t_{spent}=\int_0^{t_{max}}\left(\int_{region}|\psi(x,z,t)|^2 dz\,dx\right)dt, \qquad (1)$$

are given in Table I. For $X_{apex}=2$ nm the tip is far from the NT. The wave packet is tunneling simply from the tip apex into the plane support. For $X_{apex}=0$ nm the tunneling process is more complex. t_{spent} is much longer than for $X_{apex}=2$ nm. The WP has to tunnel through two tunnel resistances[11] in series, which is characteristic to resonant tunneling. The WP first flows around the NT ($t=1.7$ fs) then penetrates into the support ($t=2.9$ fs). At later times the main mass of the probability is scattered back into the tip bulk. The probability which remained in the tube region forms standing wave patterns along the tube circumference and it is leaking into the tip and into the support in distinct impulses.[11] For $X_{apex}=0.8$ nm the majority of the probability flows out of the tip at its side. For $X_{apex}=1.6$ nm we can observe the switching of the tunneling point from the side to the apex of the tip.

The STM constant current loop was simulated by finding for each X_{apex} lateral tip displacement that Z_{apex} vertical tip displacement that yielded a constant tunneling probability. This set-point probability was chosen to be 3×10^{-3} and it gave a 0.4093-nm separation between the tip and NT geometrical surfaces (at $X_{apex}=0$ nm). The (X_{apex}, Z_{apex}) tip displacement values resulting from this procedure give the QLC, which is shown in Fig. 1 with crosses.

The comparison of simulation and experiment shows that when the NT is placed on a support with a similar electronic structure, the GLC coincides with the QLC (cf. Fig. 1). The major distortion that influences the apparent tube diameter is the geometric convolution of the tip shape with the tube shape. When the NT is on a support with different electronic properties, the simplification used in the QLC calculation: the penetration and propagation parameters (E_F and W) of the WP in the NT and in the support is identical, is not any more valid. In the case of the GLC this can be taken in account in the first approximation by increasing the value of the tunnel gap over the support as compared to the value over the NT. This will increase the distortion found in the apparent diameter of the NT with increasing difference in the electronic structure of the NT as compared to graphite. The ratio of half-width HW to height h versus the increase of the width of the tunnel gap over the support is shown in Fig. 3. Comparing the case of the NT over the raft,[10] i.e., identical electronic structure, with Fig. 3, one may conclude that in the experimental case the distortion agrees within the experimental error with the value corresponding to zero tunnel gap increase in the figure. When performing $I(V)$ spectroscopy, one has the response of a complex system to the changes of the voltage applied to the tunnel gap. This is shown by the differences in the average times (cf. Table I) spent in the different regions. Therefore, the interpretation of the $I(V)$ curve may be a more complex task than can be achieved with the methods commonly used in the interpretation of STS results measured on well-ordered single crystalline surfaces.

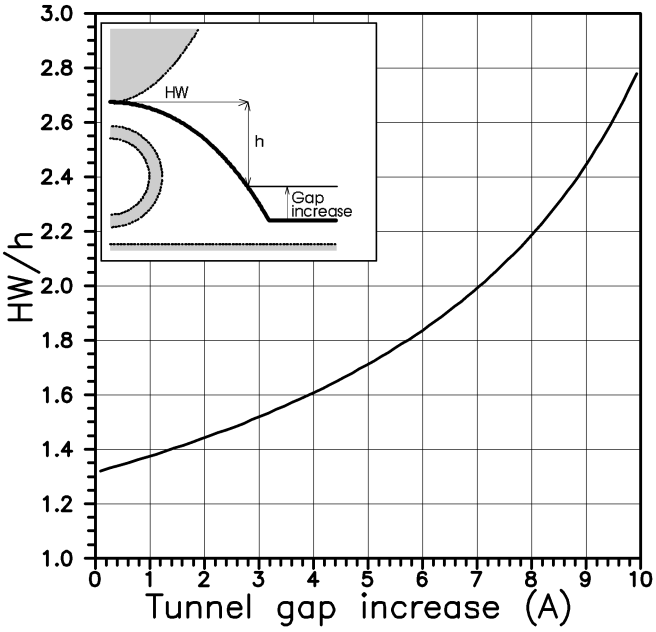

FIG. 3. HW/h versus the increase of the tunneling gap above the support. Definitions of HW, h, and the gap increase are given on the GLC shown in the inset.

In conclusion, as long as the electronic structure of the NT and of its support are similar, the major distortion arises from the geometric convolution. This is found experimentally in the case of NT's placed on the top of rafts of similar NTs. When the electronic structure of the support is different from that of the NT, i.e., when HOPG, gold, or other support is used, further distortions arise from the modification of the width of the tunnel gap over the NT if compared to the value found over the support. The existence of the second tunnel gap, between the NT and its support may introduce complications in the interpretation of STS data. Our present model does not take in account the particular electronic structure of the NT itself, so differences between semiconducting and metallic NT's cannot be accounted for but we are given a kind of average behavior. Further work is needed, to realize a more rigorous description of the tunneling through a supported NT.

Helpful discussions with Professor Ph. Lambin of FUNDP, Namur, are gratefully acknowledged. This work was partly supported by AKP Grant No. 96/2-637. G.I.M. is indebted to Professor E. Balázs for constant support.

*Electronic address: mark@sunserv.kfki.hu

[1] M. S. Dresselhaus, G. Dresselhaus, and P. C. Eklund, *Science of Fullerenes and Carbon Nanotubes* (Academic Press, San Diego, 1996).
[2] Ph. Lambin, A. Fonseca, J. P. Vigneron, J. B. Nagy, and A. A. Lucas, Chem. Phys. Lett. **245**, 85 (1995).
[3] C. H. Olk and J. P. Heremans, J. Mater. Res. **9**, 259 (1994).
[4] M. Ge and K. Sattler, Science **260**, 515 (1993).
[5] S. Xie, N. Li, Z. Zhang, W. Lu, G. Wang, S. Qian, and C. Fu, J. Mater. Sci. **30**, 2291 (1995).
[6] N. Lin, J. Ding, S. Yang, and N. Cue, Carbon **34**, 1295 (1996).
[7] Z. Zhang and C. M. Layber, Appl. Phys. Lett. **62**, 2792 (1993).
[8] W. Rivera, J. M. Perez, R. S. Ruoff, D. C. Lorents, R. Malhotra, S. Lim, Y. G. Rho, E. G. Jacobs, and R. F. Pinizotto, J. Vac. Sci. Technol. B **13**, 327 (1995).
[9] D. L. Carroll, P. Redlich, P. M. Ajayan, J. C. Charlier, X. Blase, A. De Vita, and R. Carr, Phys. Rev. Lett. **78**, 2811 (1997).
[10] L. P. Biró, S. Lazarescu, Ph. Lambin, P. A. Thiry, A. Fonseca, J. B. Nagy, and A. A. Lucas, Phys. Rev. B **56**, 12 490 (1997).
[11] L. P. Biró, J. Gyulai, Ph. Lambin, J. B. Nagy, S. Lazarescu, G. I. Márk, A. Fonseca, P. R. Surján, Zs. Szekeres, P. A. Thiry, and A. A. Lucas, Carbon **36**, 689 (1998); http://www.phy.bme.hu/pub/emrs97/index.html
[12] A. Thess, R. Lee, P. Nikolaev, H. Dai, P. Petit, J. Robert, C. Xu, Y. H. Lee, S. G. Kim, A. G. Rinzler, D. T. Colbert, G. E. Scuseria, D. Tomanek, J. E. Fischer, and R. E. Smalley, Science **273**, 483 (1996).
[13] P. Sautet, J. Dunphy, D. F. Ogletree, and M. Salmeron, Surf. Sci. **295**, 347 (1993).
[14] J. Cerdá, M. A. Van Hove, P. Sautet, and M. Salmeron, Phys. Rev. B **56**, 15 885 (1997).
[15] D. Östling, D. Tománek, and A. Rosén, Phys. Rev. B **55**, 13 980 (1997).
[16] J. C. Boettger, Phys. Rev. B **55**, 11 202 (1997).
[17] Landolt-Börnstein, *Eigenschaften der Materie in ihren Aggregatzuständen, 6. Teil: Elektrische Eigenschaften I* (Springer, Berlin, 1959), p. 914.
[18] J. A. Fleck, J. R. Morris, and M. D. Feit, Appl. Phys. **10**, 129 (1976).
[19] M. D. Feit, J. A. Fleck, and A. Steiger, J. Comput. Phys. **47**, 412 (1982).
[20] G. I. Márk and P. Pacher, in *Proceedings of the International Conference on Mathematical Methods in Science and Technology, 3-6 June 1995, Vienna*, edited by W. Kainz (University of South Bohemia, České Budějovice, 1995), p. 59.
[21] A. Goldberg, H. M. Schey, and J. L. Schwartz, Am. J. Phys. **35**, 177 (1967).
[22] C. R. Leavens and G. C. Aers, Phys. Rev. B **39**, 1202 (1989).